Properties of Quasi-local mass in binary black hole mergers

Daniel Pook-Kolb,[1, 2, 3, *] Bowen Zhao,[4, †] Lars Andersson,[4, ‡] Badri Krishnan,[1, 2, 3, §] and Shing-Tung Yau[4, 5, ¶]

[1]*Institute for Mathematics, Astrophysics and Particle Physics,*
Radboud University, Heyendaalseweg 135, 6525 AJ Nijmegen, The Netherlands
[2]*Albert-Einstein-Institut, Max-Planck-Institut für Gravitationsphysik, Callinstraße 38, 30167 Hannover, Germany*
[3]*Leibniz Universität Hannover, 30167 Hannover, Germany*
[4]*Beijing Institute of Mathematical Sciences and Applications, Beijing 101408, China*
[5]*Yau Mathematical Sciences Center, Tsinghua University, Beijing 100084, China*
(Dated: August 23, 2023)

Identifying a general quasi-local notion of energy-momentum and angular momentum would be an important advance in general relativity with potentially important consequences for mathematical and astrophysical studies in general relativity. In this paper we study a promising approach to this problem first proposed by Wang and Yau in 2009 based on isometric embeddings of closed surfaces in Minkowski space. We study the properties of the Wang-Yau quasi-local mass in high accuracy numerical simulations of the head-on collisions of two non-spinning black holes within full general relativity. We discuss the behavior of the Wang-Yau quasi-local mass on constant expansion surfaces and we compare its behavior with the irreducible mass. We investigate the time evolution of the Wang-Yau Quasi-local mass in numerical examples. In addition we discuss mathematical subtleties in defining the Wang-Yau mass for marginally trapped surfaces.

I. INTRODUCTION

The quasi-local definition of energy-momentum remains one of the major problems in classical general relativity [1, 2]. The goal is to find appropriate notions of energy-momentum and angular momentum for finite, extended regions of spacetime. At spatial infinity and at null infinity, there are well-established concepts of energy and angular momentum. The energy-momentum defined by Arnowitt-Deser-Misner (ADM) [3] at spatial infinity measures the *total* energy in a spacetime, and it is conserved and shown to be positive [4, 5]. The Bondi energy is measured at null-infinity and satisfies appropriate balance laws as gravitational radiation carries away energy and angular momentum [6]. Similarly, there are notions of quasi-local energy and angular momentum and balance laws applicable for black hole horizons [7–9]. In contrast, finding suitable analogous definitions for a finitely extended body or for an arbitrary region in spacetime is still under active research.

Finding appropriate quasi-local notions of energy momentum and angular momentum would be desirable for various reasons. For example, one might expect that gravitational waves emitted from a given region in spacetime would carry away energy thus leading to a corresponding decrease in the quasi-local mass. Such a link has been shown for the Bondi mass and for black hole horizons, but is still not available for general spacetime regions. Once fully understood, it could potentially allow us to infer detailed properties of dynamical spacetimes in the strong field region from gravitational wave observations, such as from the merger of compact objects. On the mathematical side, it is likely that appropriate quasi-local notions of energy and angular momentum would play an important role in providing a full proof of the Penrose inequality. Similarly, as we shall discuss in this paper, quasi-local mass also plays an important role in the process of gravitational collapse and black hole formation via the hoop conjecture.

We expect quasi-local mass to be a flux type integral on a closed space-like 2-surface Σ which bounds a space-like hypersurface Ω. Since Ω is not unique in the sense of being bounded by a given Σ, one would expect that a proper notion of quasi-local mass should not depend on which specific Ω is chosen. Restricting ourselves to vacuum spacetimes, we can enumerate some minimal requirements that any viable notion of quasi-local mass $M_{(\Sigma)}$ should satisfy [10]:

- In flat Minkowski spacetime, $M_{(\Sigma)}$ should vanish.

- In a curved spacetime, the quasi-local mass should be non-negative.

- In the limit when Σ approaches a sphere at space-like infinity on an asymptotically flat slice, or a cross-section of null infinity, the quasi-local mass must approach the ADM mass or the Bondi mass, respectively.

- When Σ is an apparent horizon, the quasi-local mass must be bounded from below by the irreducible mass of Σ, i.e. $\sqrt{A_\Sigma/16\pi}$, where A_Σ is the area of Σ.

In this work we shall investigate properties of the quasi-local mass originally proposed by Wang & Yau [11]; see also [12]. There are several other proposed definitions

---

* daniel.pook.kolb@aei.mpg.de
† bowenzhao@bimsa.cn
‡ lars.andersson@bimsa.cn
§ badri.krishnan@ru.nl
¶ styau@tsinghua.edu.cn

of quasi-local mass, energy-momentum and angular momentum in the literature. Some notable ones are due to Bartnik [13], Hawking [14], and Penrose [15]; see [1, 2] for a review.

Based on a variational analysis of the action of General Relativity, Brown & York proposed a quasi-local energy arising as a boundary term in the Hamiltonian [16, 17]; see also [10, 12, 18]. However, the Brown-York definition depends explicitly on a choice of spacelike hypersurface Ω that is bounded by the two-surface Σ under consideration. Specifically, the mean curvature of Σ as embedded in Ω appears in the Brown-York definition. Moreover, a specific choice of unit lapse and zero shift is needed in relating the Hamiltonian to the Brown-York mass. This rather arbitrary gauge-fixing is undesirable in general relativity studies. Furthermore, the Brown-York quasi-local mass can fail to be positive in general except for the time symmetric case [19]. On the other hand, there exist surfaces in Minkowski spacetime with strictly positive Brown-York mass. These undesirable features are resolved in Wang & Yau [20] by further including momentum information (second fundamental form in the time direction) in their definition. Indeed, Euclidean space can be regarded as the totally geodesic space-like hypersurface of zero momentum in Minkowski spacetime. While Brown & York defined their reference surface by an isometric embedding of Σ into 3-dimensional Euclidean space $\mathbb{R}^3$, Wang & Yau defined their reference surface by an isometric embedding into Minkowski space $\mathbb{R}^{3,1}$ directly. The positivity proof of Wang-Yau quasilocal mass is given along with the definition [20]. The new definition is proven to recover the ADM mass at spatial infinity [21] and the Bondi mass at null infinity [22]. Further, the small sphere limit is proven to recover the stress-energy tensor at the limiting point for a spacetime with matter fields and is related to the Bel–Robinson tensor at higher orders for vacuum spacetime. Along the same line, they also give a quasi-local definition for angular momentum and center of mass [23], which are proven to be super-translation invariant [24–26]. We will review the definition of Wang & Yau quasi-local mass below and compare with Brown & York when it is helpful.

Besides the requirements enumerated above, additional properties would be desirable when considering the dynamical aspects of general relativity. As mentioned earlier, for the Bondi mass at null infinity, the Bondi mass loss formula shows that gravitational waves carry away energy, leading to a decrease of the Bondi mass [6]. The flux of gravitational radiation is written as a surface integral over cross-sections of null infinity, and is manifestly positive. Similarly, restricting ourselves to black hole horizons and marginally trapped surfaces, similar balance laws with positive fluxes can be shown, leading to a physical process version of the area increase law [7–9]. Extending these considerations to a more general quasi-local setting would lead one to conjecture that the emission (or absorption) of gravitational radiation from a domain Ω could be written as a surface flux integral

over Σ, directly related to the decrease (or increase) of the quasi-local mass. At present we do not have a well defined notion of such fluxes. As a first step in this direction, in this work we shall study the time evolution of Wang-Yau quasi-local mass, henceforth denoted as QLM, in the context of a binary black hole merger. This question is hard to answer analytically, and we resort instead to high precision numerical simulations of the full Einstein equations.

The plan for this paper is the following. The basics of the Wang-Yau QLM and its properties are introduced in Sec. II. We shall consider the head-on collision of two non-spinning black holes starting with time-symmetric initial data. The initial data and our numerical evolution scheme is described in III. Our numerical implementation for calculating the Wang-Yau QLM, and numerical convergence, are described in Sec. IV. The numerical results are presented in Sec. V in three steps. First, Sec. V A shows the results in the initial data, i.e. with time symmetry. As the evolution proceeds, the later time slices are no longer time-symmetric. Sec. V B shows results for non-time-symmetric slices and finally Sec. V C presents the time evolution of the QLM and also an exploration of the hoop conjecture in the context of the formation of the common horizon in a black hole merger. In the course of presenting the numerical results, it will be clear that there are mathematical subtleties in defining the QLM for a marginally trapped surface. This will be clarified mathematically in Sec. VI and will justify the various choices made in the numerical work. Finally, Sec. VII will discuss some implications of our results and suggestions for future work.

II. BASIC NOTIONS

The Wang-Yau quasi-local energy (QLE) associated with a suitable surface is defined through anchoring the surface intrinsic geometry while comparing the extrinsic geometry as embedded in the original spacetime $\mathcal{N}^4$ versus that embedded in the flat Minkowski space $\mathbb{R}^{3,1}$. Given a spacelike two-surface $\Sigma \subset \mathcal{N}^4$ with induced metric σ_{ab}, let $i_0 : \Sigma \hookrightarrow \mathbb{R}^{3,1}$ be an isometric embedding into the Minkowski spacetime. Fixing a unit, future-pointing, timelike vector T_0 in $\mathbb{R}^{3,1}$, a one-to-one correspondence between vector fields in $\mathcal{N}^4$ and those in $\mathbb{R}^{3,1}$ is built through the 'canonical gauge' condition,

$$\langle H, \bar{e}_4 \rangle = \langle H_0, \check{e}_4 \rangle , \qquad (1)$$

where H and H_0 are mean curvature vectors of $\Sigma \subset \mathcal{N}^4$ and $i_0(\Sigma) \subset \mathbb{R}^{3,1}$, respectively, and $\langle \cdot, \cdot \rangle$ denotes the corresponding scalar product in $\mathcal{N}^4$ and $\mathbb{R}^{3,1}$. The basis vectors $\bar{e}_\alpha$ of $\mathcal{N}^4$, $\alpha \in \{0, 1, 2, 3\}$, and $\check{e}_\alpha$ of $\mathbb{R}^{3,1}$ are chosen as follows. Let $\check{e}_3$ be the spacelike unit normal of $i_0(\Sigma)$ which is also perpendicular to T_0. Let $\check{e}_4$ be the future-pointing, timelike unit normal that is perpendicular to $\check{e}_3$. Then $\{\check{e}_3, \check{e}_4\}$ forms an orthonormal basis for the normal bundle of $i_0(\Sigma) \subset \mathbb{R}^{3,1}$. The canonical gauge

condition (1) picks uniquely a future-pointing, timelike unit normal of Σ, $\bar{e}_4$. Then $\bar{e}_3$ is the spacelike normal of Σ that combined with $\bar{e}_4$ gives an orthonormal basis for the normal bundle of $\Sigma \subset \mathcal{N}^4$.

Given $\tau \in C^\infty(\Sigma)$, a generalized mean curvature for Σ is defined as

$$\mathcal{H} = -\sqrt{1 + |\nabla\tau|^2}\langle H, \bar{e}_3 \rangle - \alpha_{\bar{e}_3}(\nabla\tau) , \qquad (2)$$

where ∇ denotes the covariant derivative on Σ associated with σ_{ab}, $|\nabla\tau|^2 = \sigma^{ab}\nabla_a\tau\nabla_b\tau$ and we write $\alpha_{\check{e}_3}(\nabla\tau) = (\alpha_{\check{e}_3})_a\nabla^a\tau$. The connection one-form $\alpha_{\bar{e}_3}$ associated with the basis $\{\bar{e}_3, \bar{e}_4\}$ is defined as

$$\alpha_{\bar{e}_3}(Y) = \langle {}^{(4)}\nabla_Y \bar{e}_3 , \bar{e}_4 \rangle ,$$

where $Y \in T\Sigma$ and ${}^{(4)}\nabla$ denotes the covariant derivative in $\mathcal{N}^4$. Similarly, one can define $\alpha_{\check{e}_3}$ for the connection one-form associated with $\{\check{e}_3, \check{e}_4\}$ in $\mathbb{R}^{3,1}$ as

$$\alpha_{\check{e}_3}(Y) = \langle {}^{(3,1)}\nabla_Y \check{e}_3 , \check{e}_4 \rangle ,$$

where ${}^{(3,1)}\nabla_Y$ denotes the covariant derivative in $\mathbb{R}^{3,1}$. A generalized mean curvature for $i_0(\Sigma)$ is defined as

$$\mathcal{H}_0 = -\sqrt{1 + |\nabla\tau|^2}\langle H_0, \check{e}_3 \rangle - \alpha_{\check{e}_3}(\nabla\tau) . \qquad (3)$$

The Wang-Yau quasi-local energy associated with τ is then defined as

$$\mathrm{QLE}(\tau) = \frac{1}{8\pi}\int_\Sigma (\mathcal{H}_0 - \mathcal{H})\, dvol_\Sigma . \qquad (4)$$

When the mean curvature vector H is spacelike, one can use $H = -\langle H, \bar{e}_4 \rangle \bar{e}_4 + \langle H, \bar{e}_3 \rangle \bar{e}_3 = p\,\bar{e}_4 - k\,\bar{e}_3$ and its conjugate vector $J = k\,\bar{e}_4 - p\,\bar{e}_3$ to form an orthonormal basis for the normal bundle $N\Sigma$, $\{e_H = -\frac{H}{|H|}, e_J = \frac{J}{|H|}\}$. In terms of this mean curvature vector basis,

$$\mathrm{QLE}(\tau) =$$
$$\frac{1}{8\pi}\int_\Sigma \left\{ \sqrt{1 + |\nabla\tau|^2} \cdot (\cosh\theta_0 |H_0| - \cosh\theta |H|) \right.$$
$$\left. - \nabla\tau \cdot \nabla(\theta_0 - \theta) - (\alpha_{H_0} - \alpha_H)(\nabla\tau) \right\} ,$$

where θ denotes the hyperbolic angle between $\{\bar{e}_3, \bar{e}_4\}$ and $\{e_H = -\frac{H}{|H|}, e_J = \frac{J}{|H|}\}$. Specifically,

$$\begin{cases} \bar{e}_3 = \cosh\theta\, e_H - \sinh\theta\, e_J \\ \bar{e}_4 = -\sinh\theta\, e_H + \cosh\theta\, e_J \end{cases} \qquad (5)$$

and similarly for θ_0 in $\mathbb{R}^{3,1}$.

Solving the variational problem of minimizing the QLE with respect to the time function τ, one gets the Euler-Lagrange equation, called the optimal embedding equation (OEE),

$$\nabla_a j^a = 0 . \qquad (6)$$

The minimum value of QLE is defined to be the Wang-Yau quasi-local mass

$$\mathrm{QLM} = \frac{1}{8\pi}\int_\Sigma \rho + j^a\nabla_a\tau = \frac{1}{8\pi}\int_\Sigma \rho , \qquad (7)$$

where (see (4.4)–(4.5) in [27] for details)

$$\rho = \frac{\sqrt{|H_0|^2 + \frac{(\Delta\tau)^2}{1+|\nabla\tau|^2}} - \sqrt{|H|^2 + \frac{(\Delta\tau)^2}{1+|\nabla\tau|^2}}}{\sqrt{1 + |\nabla\tau|^2}} \qquad (8)$$

and

$$j_a = \rho\nabla_a\tau - \nabla_a \sinh^{-1}\frac{\rho\Delta\tau}{|H_0||H|} - (\alpha_{H_0})_a + (\alpha_H)_a . \qquad (9)$$

The Wang-Yau QLM is defined for any closed spacelike surface Σ whose mean curvature vector is spacelike and where an admissible solution to the OEE (6) exists (see Definition 5.1 in [20] for admissible τ).

Note that if $\tau = \mathrm{const}$ is admissible and solves the optimal embedding equation, it must be the global minimum of Wang-Yau quasi-local energy [28]. Substituting $\tau = \mathrm{const}$ to (7), one sees that the Wang-Yau quasi-local mass reduces to the Liu-Yau mass in this case [10, 12]

$$\mathrm{QLM} = \frac{1}{8\pi}\int_\Sigma |H_0| - |H| . \qquad (10)$$

If further Σ lies in a totally geodesic slice, the Wang-Yau quasi-local mass reduces to the Brown-York mass

$$m_{\mathrm{BY}} = \frac{1}{8\pi}\int_\Sigma k_0 - k , \qquad (11)$$

where k is the only nonzero component of H lying in the totally geodesic slice while k_0 is the mean curvature vector of $i_0(\Sigma)$ embedded in $\mathbb{R}^3$. Note that τ only appears through derivatives and we hence use $\tau = 0$ and $\tau = \mathrm{const}$ interchangeably.

In black hole spacetimes, there is a particular set of surfaces of interest—the marginally outer trapped surfaces (MOTSs). These are used to study various aspects of black holes quasi-locally via the framework of isolated and dynamical horizons, respectively describing black holes in equilibrium and in dynamical situations (see e.g. [29–33]). In any given spacelike slice $\mathcal{S} \subset \mathcal{N}^4$, the outermost MOTS is called the apparent horizon. Given a MOTS on a spacelike slice, the results of Andersson et al. [34–36] show the conditions under which it evolves smoothly. It is shown that when a MOTS is stable under outward deformations, then it will evolve smoothly. Recent numerical work has applied and further explored the stability of MOTSs and its implications for the time evolution [37–42].

A MOTS is defined as follows. Let $\Sigma \subset \mathcal{N}^4$ be a closed spacelike surface and let ℓ^+, ℓ^- be two future directed null normal fields on Σ taken to point outward and inward, respectively. We fix the cross normalization by

$\langle \ell^+, \ell^- \rangle = -2$, which still leaves a remaining freedom to scale

$$\ell^+ \to f\ell^+ \,, \qquad\qquad \ell^- \to \frac{1}{f}\ell^- \qquad (12)$$

for any positive function f. The outward and inward null expansions, denoted Θ_+ and Θ_- respectively, are defined as

$$\Theta_\pm = \sigma^{\alpha\beta}\,{}^{(4)}\nabla_\alpha \ell_\beta^\pm \,, \qquad (13)$$

where $\sigma^{\alpha\beta} = \sigma^{ab}\pi_a^\alpha\pi_b^\beta$ with π_a^α the projection onto the tangent bundle of Σ. Then, Σ is called a *marginally outer trapped surface* (MOTS) if $\Theta_+ = 0$, an *outer trapped surface* if $\Theta_+ < 0$ and an *outer untrapped surface* if $\Theta_+ > 0$. A *marginally trapped surface* (MTS) is a MOTS with $\Theta_- < 0$. Note that although $\Theta_\pm \to f\Theta_\pm$ under (12), the signs of $\Theta_\pm$ are invariant and so these definitions are not affected.

We will often consider families of surfaces Σ_s with constant $\Theta_+ = s \in \mathbb{R}$, called *constant expansion surfaces* (CESs). These do depend on the choice of $\ell^\pm$, which we fix uniquely using the spacelike slice $\mathcal{S} \subset \mathcal{N}^4$ within which the family Σ_s is constructed. Concretely, let $\Sigma_s \subset \mathcal{S}$, v the spacelike outward unit normal of Σ_s in $\mathcal{S}$ and u the future timelike unit normal on $\mathcal{S}$ in $\mathcal{N}^4$. Then, we choose

$$\ell^\pm = u \pm v \,. \qquad (14)$$

In terms of the null expansions $\Theta_\pm$, the mean curvature vector H and its conjugate vector J can be expressed as

$$H = \frac{\Theta_+\ell^- + \Theta_-\ell^+}{2} \,, \quad J = \frac{\Theta_+\ell^- - \Theta_-\ell^+}{2} \,. \quad (15)$$

Since $\langle H, H \rangle = -\Theta_+\Theta_-$, the mean curvature vector becomes a null vector on a MOTS. If in addition the slice $\mathcal{S}$ is time symmetric, i.e. its second fundamental form vanishes, then $\sigma^{\alpha\beta}\,{}^{(4)}\nabla_\alpha u_\beta = 0$ and thus $\Theta_+ = -\Theta_-$ implying that H and J both vanish on a MOTS.

To characterize the quasi-local mass of a black hole region, we take the QLM of apparent horizons. However, the current definition of the Wang-Yau quasi-local mass assumes the surface mean curvature vector to be spacelike and hence does not apply to MOTSs. Therefore, one of our goals is to extend the definition of the Wang-Yau QLM (7) to a MOTS in time symmetry and to an MTS without time symmetry. Limiting ourselves to the case of axisymmetry and no angular momentum, we will argue that a suitable extension is

$$\text{QLM} = \frac{1}{8\pi}\int_\Sigma |H_0| \qquad \text{with } \tau = \text{const}\,. \qquad (16)$$

With this extension, we can then investigate the time evolution of QLM during black hole collisions. As noted above if Σ lies in a totally geodesic slice, e.g. in the moment of time-symmetry, Wang-Yau QLM reduces to

Brown-York mass. In this case, the above extension simply reduces to QLM $= \frac{1}{8\pi}\int k_0$, which is what one would expect for the Brown-York limit at minimal surfaces. Further extension of QLM to surfaces of timelike mean curvature vector, e.g. trapped surfaces inside event horizons, is certainly of great interest and will be studied elsewhere.

III. INITIAL DATA AND NUMERICAL EVOLUTION

We use Brill-Lindquist initial data [43], which solves the constraint equations of General Relativity with vanishing extrinsic curvature and vanishing scalar curvature, i.e. a time-symmetric slice in vacuum spacetime. The Riemannian three-metric is defined on $\mathbb{R}^3 \setminus \{x_1, \dots, x_n\}$ with $n+1$ asymptotically flat ends, one at $\|x\| \to \infty$ and n at the punctures x_i. We restrict ourselves to the case $n = 2$, which describes a two-black-hole configuration. The three-metric can then be written as

$$h_{ij} = \Phi^4 \delta_{ij} \,, \qquad (17)$$

where δ_{ij} is the flat metric and the conformal factor is

$$\Phi = 1 + \frac{m_A}{2|x - x_A|} + \frac{m_B}{2|x - x_B|} \,. \qquad (18)$$

We take the two punctures to be located on the z-axis at coordinates $x_{A,B} = (0, 0, \pm d/2)$, respectively. The three ends at $\|x\| \to \infty$, x_A and x_B, respectively, have ADM-masses

$$M^{\text{ADM}} = m_A + m_B \,, \qquad (19)$$

$$M_A^{\text{ADM}} = m_A + \frac{m_A\,m_B}{2d} \,, \qquad (20)$$

$$M_B^{\text{ADM}} = m_B + \frac{m_A\,m_B}{2d} \,. \qquad (21)$$

For sufficiently large d, the slice $\mathcal{S}$ contains two separate black holes, each surrounded by a stable MOTS that contains either x_A or x_B. We shall call these the *individual MOTSs* Σ_A and Σ_B, respectively. If d becomes small enough, there exists a stable common MOTS Σ_{outer} surrounding $\Sigma_{A,B}$. In fact, as d passes through the value at which Σ_{outer} appears, it is found that an unstable MOTS Σ_{inner} forms together with Σ_{outer} and "moves" inward as d is decreased. This is discussed in more detail elsewhere [44].[1] The two common and two individual MOTSs for an equal mass configuration are shown in Fig. 1.

The numerical data for this initial slice are generated by the *TwoPunctures* [45] thorn of the *Einstein Toolkit* [46, 47]. These data are evolved in time using an axisymmetric version of *McLachlan* [48], which in turn uses

----

[1] There is a large number of additional MOTSs in these data [40–42], which are all found to be unstable. We will hence not discuss these surfaces in the present work.
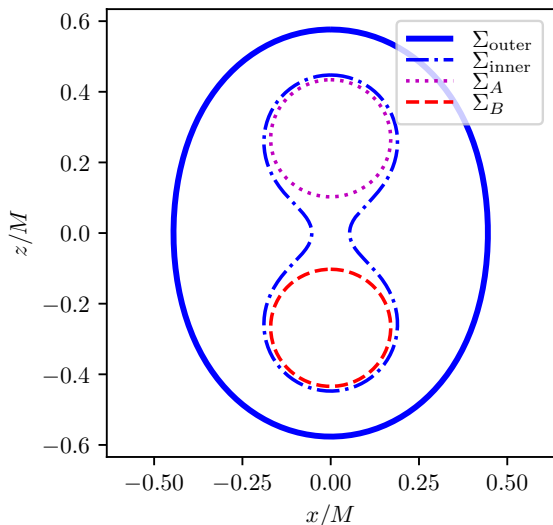
FIG. 1. Common MOTS Σ_{outer}, inner common MOTS Σ_{inner} and the two individual MOTSs Σ_A and Σ_B in Brill-Lindquist initial data with parameters $m_A = m_B = d = 1/2$.

Kranc [49, 50] for generating C++ code. This uses the BSSN formulation of the Einstein equations with gauge conditions chosen as the so-called $1+\log$ slicing and a Γ-driver shift condition [51, 52]. More details about our numerical simulation setup, including a convergence analysis, are described in [38].

Our analysis is based on two simulations, both starting from BL data. The first, referred to as Sim1, uses initial data with $m_B/m_A = 2, d = 0.9$ and the second, simulation Sim2, uses $m_B/m_A = 1.6, d = 1$. Both simulations were performed with different spatial grid resolutions to check the accuracy of our calculations. Results shown for Sim1 use a resolution $1/\Delta x = 720$, which was evolved until simulation time $t_f = 6$. For Sim2, we used a lower resolution of $1/\Delta x = 312$ to extend the evolution up to time $t_f = 38$.

The MOTSs and CESs are numerically found with high accuracy both in the analytical initial data as well as in slices produced by the *Einstein Toolkit* using the method in [44, 53].

In general, the problem of locating a surface Σ_s with expansion $\Theta_+ = s$ may have many solutions within a given slice $\mathcal{S}$. For $s = 0$, this corresponds to the different MOTSs in $\mathcal{S}$. By choosing suitable initial guesses for the numerical search, we can easily select which particular MOTS to find. As mentioned above, we focus here on the three stable MOTSs Σ_{outer}, Σ_A and Σ_B, interpreted as the horizon of the merger remnant and the smaller and larger (in case of unequal masses) individual black holes. Choosing one of these MOTSs as initial guess, we construct CESs for s close to zero. Families of Σ_s are then built by taking small steps in s, each time using the previous CES as initial guess for the next. CESs far from Σ_{outer} in the nearly flat region of $\mathcal{S}$ are close

to being spherical in our coordinates and so we can use coordinate spheres as initial guesses in this case.

IV. NUMERICAL METHOD FOR EVALUATING THE QUASI-LOCAL MASS

The strategy to solve the optimal embedding equation $\nabla_a j^a = 0$ is to consider $\nabla_a j^a$ as a nonlinear operator $\mathcal{L}$ acting on τ, linearize that operator $\mathcal{L}$ and solve the linear problem multiple times, each time taking a small step towards a solution of the full nonlinear problem. This is also called the *Newton-Kantorovich* method [54, Appendix C].

Analytically linearizing $\mathcal{L}$ requires determining the explicit dependency of $\nabla_a j^a$ on τ. We make use of axisymmetry, i.e. assuming the surface Σ, the embedding i_0 and τ are all axisymmetric, to simplify calculations. The time function τ then depends only on one parameter, say θ, increasing from one pole of Σ to the other, and the embedding i_0 can be expressed in terms of the intrinsic metric σ_{ab} and τ', where $\tau' = \frac{d\tau}{d\theta}$. Explicitly, for coordinates $\{y^1 = \theta, y^2 = \phi\}$ on Σ, $0 < \theta < \pi$ and $0 < \phi < 2\pi$, an axisymmetric ansatz for the embedding is

$$i_0(\theta, \phi) = \begin{pmatrix} \tau(\theta) \\ R(\theta)\cos\phi \\ R(\theta)\sin\phi \\ Z(\theta) \end{pmatrix}. \quad (22)$$

Writing the two-metric as $d\sigma^2 = P^2 d\theta^2 + Q^2 \sin^2\theta \, d\phi^2$, we then have

$$R^2 = Q^2 \sin^2\theta\,, \qquad Z'^2 = P^2 - V'^2 + \tau'^2\,, \quad (23)$$

where $V = Q\sin\theta$. Using this, we calculate $\langle H_0, H_0 \rangle = k_0^2 - p_0^2$ via

$$k_0 = \frac{VV''Z' - P^2 Z' + VV'Z''}{\sqrt{P^2 + \tau'^2}P^2 V}\,, \quad (24)$$

$$p_0 = \frac{P'V\tau' - P(V\tau'' + V'\tau')}{\sqrt{P^2 + \tau'^2}P^2 V}\,. \quad (25)$$

Furthermore,

$$(\alpha_{H_0})_\theta = \frac{k_0 p_0' - p_0 k_0'}{|H_0|^2} + \tau'\frac{V'Z'' - V''Z'}{P(P^2 + \tau'^2)}\,. \quad (26)$$

The respective terms in curved space are calculated differently using the null expansions, which we have in highly accurate form from the MOTS and CES finding process. In addition to (15), we use

$$(\alpha_H)_a = \frac{1}{2}\left(\frac{\Theta_{,a}^+}{\Theta_+} - \frac{\Theta_{,a}^-}{\Theta_-} - \ell_+^\mu \pi_a^{\nu(4)}\nabla_\nu \ell_\mu^-\right)\,, \quad (27)$$

where $\Theta_{,a}^\pm = \frac{\partial\Theta_\pm}{\partial y^a}$. We remark that $\Theta_\pm$ contains first derivatives of the 3-metric, which means that $\nabla_a j^a$ contains third derivatives. In order to get numerically accurate results, we expand $\Theta_\pm$ into a set of basis functions and differentiate these directly.
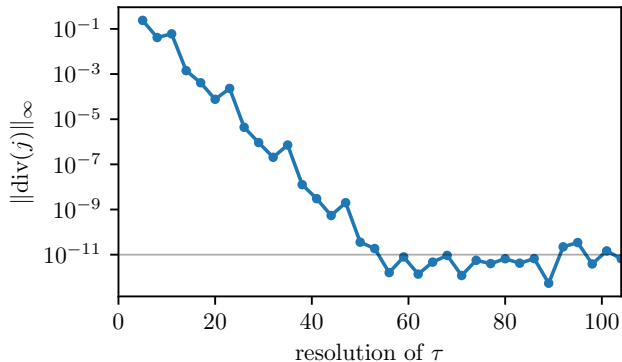
FIG. 2. Maximum residual of the OEE (6) as the resolution of our representation of τ is increased. The error drops exponentially up to reaching a numerical roundoff at about 10^{-11}. The case shown here is for a CES with $\Theta_+ \approx 0.114$ in a non-time-symmetric slice.

To linearize the operator $\mathcal{L}\tau = \nabla_a j^a$, the above expressions are first inserted in turn into (8), (9) and $\nabla_a j^a$. Afterwards, we use $SymPy$ [55] to symbolically differentiate $\mathcal{L}$ with respect to τ', τ'', $\tau^{(3)}$ and $\tau^{(4)}$. In the end, the linearized operator we implement into our numerical code is of the form

$$(\delta\mathcal{L})\Delta = \sum_{n=1}^{4} (\delta_{\tau^{(n)}}\mathcal{L}) \frac{\partial^n \Delta}{\partial \theta^n} , \qquad (28)$$

where Δ is a scalar function on Σ. Starting with an initial guess τ_0, usually $\tau_0 = 0$, we perform steps $\tau_{i+1} = \tau_i + \Delta_i$, where Δ_i solves the linear equation

$$(\delta\mathcal{L})\Delta_i = -\mathcal{L}\tau_i , \qquad (29)$$

which we solve using a pseudospectral method. In most cases, it took between 5 and 15 steps to converge up to numerical roundoff. Fig. 2 shows that the residual of the OEE (6) decreases exponentially with the resolution of τ, where the resolution is the number of basis functions used for the finite representation of τ.

V. NUMERICAL RESULTS

A. The QLM in time-symmetric initial data

For a time-symmetric slice $\mathcal{S}$, the mean curvature vector H of Σ lies in $\mathcal{S}$. A MOTS therefore coincides with a minimal surface ($k = -\langle H, v \rangle = 0$, where, as before, v is the outward unit normal of Σ in $\mathcal{S}$). Moreover, in time symmetry we have $\alpha_H = -\langle^{(4)}\nabla e_J, e_H \rangle \equiv 0$ since e_H lies in $\mathcal{S}$ while e_J is the normal to the totally geodesic slice $\mathcal{S}$. And for $\tau = \text{const}$, $i_0(\Sigma) \subset \mathbb{R}^3$, by a similar argument, $\alpha_{H_0} \equiv 0$. Thus $\tau = \text{const}$ trivially solves the optimal embedding equation (6). Furthermore, $\tau = \text{const}$ is known to be the global minimum of the QLE provided that it

solves the optimal embedding equation [28]. The Wang-Yau quasi-local mass reduces to the Brown-York mass m_{BY} for any surface Σ in a moment of time symmetry.

1. On the monotonicity along geometric flows

It is well known that for some cases, the Brown-York mass exhibits a monotonically decreasing behavior [56]. As an example, consider a Schwarzschild black hole. In a time-symmetric slice, with the metric in isotropic coordinates

$$ds^2 = \left(1 + \frac{m}{2r}\right)^4 \left(dr^2 + r^2 d\Omega^2\right) , \qquad (30)$$

the horizon lies at $r = m/2$. One can show that

$$m_{\text{BY}}\left(r = \frac{m}{2}\right) = 2m > m_{\text{BY}}(r = \infty) = m .$$

This is interpreted as negative gravitational field energy bringing down m_{BY} as the surface approaches infinity [2].

In fact, this monotonicity property could be shown more precisely. Consider two mean convex surfaces in $\mathcal{S}$, $\Sigma_i = \partial\Omega_i$, $i \in \{1, 2\}$, with $\Omega_1 \subset \Omega_2$ and suppose there exists a geometric flow

$$\frac{dF}{dt} = fv, \quad f > 0$$

from $F(t_1) = \Sigma_1$ to $F(t_2) = \Sigma_2$. Then it is proven [57, Corollary 3.3] that

$$m_{\text{BY}}(\Sigma_2) - m_{\text{BY}}(\Sigma_1)$$
$$= \frac{1}{16\pi} \int_{\Omega_2 \backslash \Omega_1} R + |B_0 - B|^2 - (k_0 - k)^2 , \quad (31)$$

where B and B_0 are the second fundamental forms of $\Sigma_t \subset \mathcal{S}$ and of $i_0(\Sigma_t) \subset \mathbb{R}^3$, respectively. For a time-symmetric slice $\mathcal{S}$, the scalar curvature $R = 2T_{00}$ and hence the $\int R$ term can be interpreted as matter contribution, which in our case vanishes. The remaining $\int |B_0 - B|^2 - (k_0 - k)^2$ term is then supposed to characterize the pure gravitational field energy. Note that although the integrand $|B_0 - B|^2 - (k_0 - k)^2$ clearly depends on the foliation Σ_t, the total integral does not. The work of Huisken & Yau [58] and later improvements [59–63] show that ends of an asymptotically flat Riemannian 3-manifold with positive ADM mass and nonnegative scalar curvature admit a unique canonical foliation through stable constant mean curvature (CMC) surfaces. The geometric flow is assured in this case with Σ_t being CMC surfaces. Nonetheless, assume (31) holds true (in our case true numerically, see below), one can discuss the sign of the gravitation field energy term. For simplicity, take an orthonormal basis for Σ_t, $\{e_1, e_2\}$, such that $\sigma_{ab} = \delta_{ab}$. This basis is also an orthonormal basis for the isometric embedding $i_0(\Sigma_t)$. Then in this basis,

$$|B_0 - B|^2 - (k_0 - k)^2 = -2\det(B_0 - B) , \qquad (32)$$
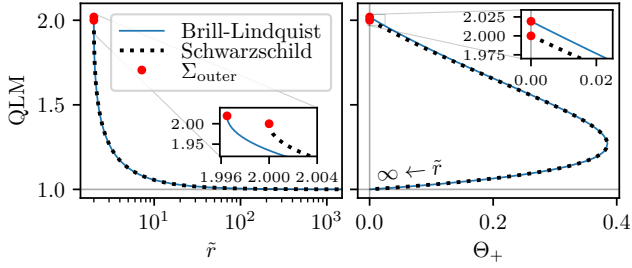
FIG. 3. QLM calculated for a family of CESs in BL data with $m_A = m_B = d = 1/2$, going from spatial infinity ($\text{QLM}_\infty = 1$) to the common horizon Σ_{outer} ($\text{QLM}_{\text{outer}} \approx 2.019209822$). The dotted line shows the QLM for constant radius surfaces in the time-symmetric Schwarzschild slice for comparison. The left panel shows the QLM as function of the area radius $\tilde{r}$, defined by $4\pi\tilde{r}^2 = A$, where A is the area, and the right panel as function of the expansion Θ_+.

where $B_0 - B = D^{\mathbb{R}^3} v_0 - Dv : T\Sigma \to T\Sigma$ is regarded as a linear map in this ON basis, with $D^{\mathbb{R}^3}$ and D denoting covariant differentiation in $\mathbb{R}^3$ and in Riemannian $\mathcal{S}$, respectively. If $B_0 - B$ can be chosen to be orientation preserving throughout a foliation Σ_t, then $\int_\Sigma |B_0 - B|^2 - (k_0 - k)^2 < 0$, i.e. it indicates negative gravitational field energy. Then m_{BY} would be monotonically decreasing as the surfaces approach infinity. We suspect this is generally true for at least mean convex Σ but a proof is missing at the moment.

We examine the above equality (31) numerically. Fig. 3 shows the QLM for CESs with $\Theta_+ \geq 0$. Outside the apparent horizon, the QLM decreases monotonically with increasing distance to the horizon, whereas the expansion $\Theta_+ = k$ increases from 0 at first (right panel, upper part) and then drops back to 0 at infinity (right panel, lower part). The balance (31) is also verified (see Fig. 4) although we cannot prove for now that there exists a geometric flow among constant expansion (mean curvature) surfaces in our case.

2. Outer trapped surfaces in time symmetry

In time symmetry, we have $\Theta_+ = -\Theta_-$ and, since

$$k = -\langle H, v \rangle = \frac{\Theta_+ - \Theta_-}{2} , \tag{33}$$

$k < 0$ everywhere for outer trapped surfaces ($\Theta_+ < 0$). However, both the Wang-Yau QLE and the Brown-York mass implicitly make the assumption that $k > 0$ and hence do not apply to such surfaces. We argue that for $k = -|H| < 0$ in the time-symmetric case, the same formula works with k replaced by its absolute value.

We first exemplify this with a time-symmetric slice of the Schwarzschild metric (30). Recall that there is an isometric inversion $r \to \frac{(m/2)^2}{r}$ that sends surfaces inside the horizon to the outside, reversing the sign of H while
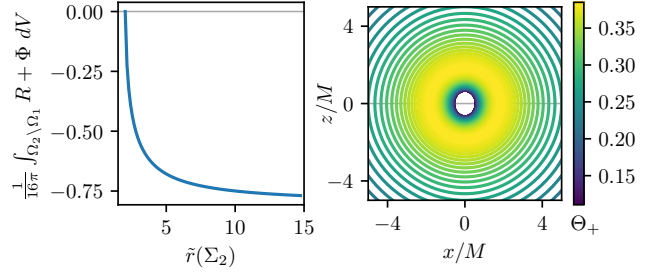

FIG. 4. Numerical evaluation of (31). The left panel shows the numerical integral, where $\Phi = |B_0 - B|^2 - (k_0 - k)^2$. It agrees with the separately computed difference $\text{QLM}(\Sigma_2) - \text{QLM}(\Sigma_1)$ to within about 10^{-7}. The x-axis represents the area radius of the outer surface Σ_2, which is varied from agreeing with Σ_1 to an almost spherical CES of area radius $\tilde{r} = 15$. The inner surface Σ_1 is a CES outside the apparent horizon with expansion $\Theta_+ = 0.1$. The right panel shows part of the CES family integrated over. The plots were produced with a Brill-Lindquist setup with $m_A = m_B = d = 1/2$.
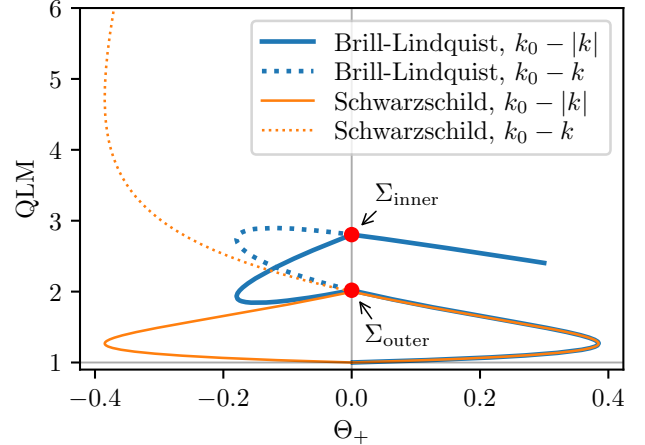

FIG. 5. Same as Fig. 3, but continuing the families to the inside of the apparent horizon in both the BL data (blue) and in a Schwarzschild slice (orange). We show a comparison of the Brown-York mass (11) calculated either via $\frac{1}{8\pi} \int_\Sigma k_0 - |k|$ (solid lines) or via $\frac{1}{8\pi} \int_\Sigma k_0 - k$ (dotted lines). For $\Theta_+ \geq 0$, the two definitions agree. In the Brill-Lindquist case, the CES family interpolates between the inner common MOTS Σ_{inner} and the apparent horizon Σ_{outer} via surfaces with $\Theta_+ < 0$. However, these latter surfaces intersect each other (Fig. 7). Monotonicity in this regime can therefore not be expected. See text for discussion.

preserving H_0 (H_0 only depends on the surface metric). Taking the absolute value of k, one has for a surface of constant radius

$$\text{QLM} = \frac{1}{8\pi} \int k_0 - |k| = \begin{cases} m(1 + \frac{m}{2r}) & r \geq \frac{m}{2} \\ 2r(1 + \frac{m}{2r}) & r \leq \frac{m}{2} \end{cases} . \tag{34}$$

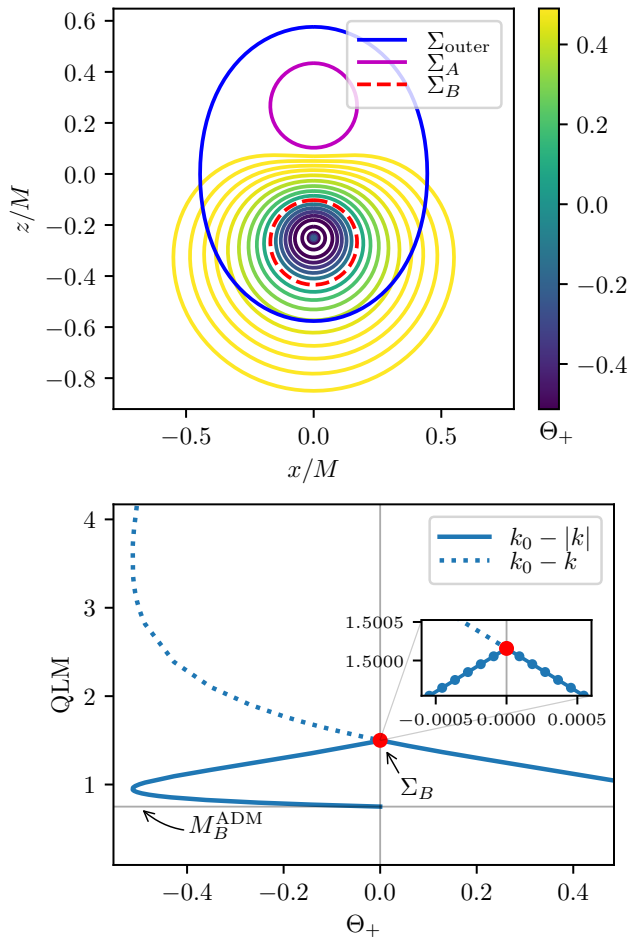This is shown in Fig. 5 (orange), where (34) is plotted together with the case of no absolute value taken (dot-

FIG. 7. Family of CESs interpolating between Σ_{outer} and Σ_{inner} in BL data with parameters $m_A = m_B = d = 1/2$. Close to Σ_{inner}, members of this family intersect each other and hence fails to foliate the space in this interior region.

FIG. 6. Upper panel: CESs near the individual MOTS Σ_B in BL data with $m_A = m_B = d = 1/2$. Lower panel: QLM calculated for these CESs. The inset shows a close-up near $\Theta_+ = 0$. As in Fig. 5, the dotted line shows (11) calculated via $\frac{1}{8\pi} \int_\Sigma k_0 - k$. The QLM asymptotes to the ADM mass 3/4 of the end at x_B as the family approaches the puncture x_B.

ted), and compared with the analogous Brill-Lindquist case (blue). Note that r denotes the isotropic radial coordinate. The QLM attains its maximum value $2m$ at the horizon while both the $r \to \infty$ and $r \to 0$ limit yield QLM $= m$, consistent with the interpretation of a time-symmetric slice in Schwarzschild as a wormhole connecting two identical, asymptotically flat regions. More specifically, for $\Theta_+ < 0$, the surface lies in the other asymptotic region, where its *outward* normal is $-v$. If we use $k < 0$ as-is, then the BY-mass remains monotonic and diverges as $\|x - x_i\| \to 0$ (i.e. approaching the other end x_i). In summary, a naive extension of Brown-York mass into the $k < 0$ region results in a smooth QLM profile while taking absolute value yields a "kink" at the horizon. In this case, a non-smooth QLM profile ($k_0 - |k|$) is clearly more natural than a smooth one ($k_0 - k$) and one might in general expect some non-analytic behavior of QLM around MOTSs or horizons.
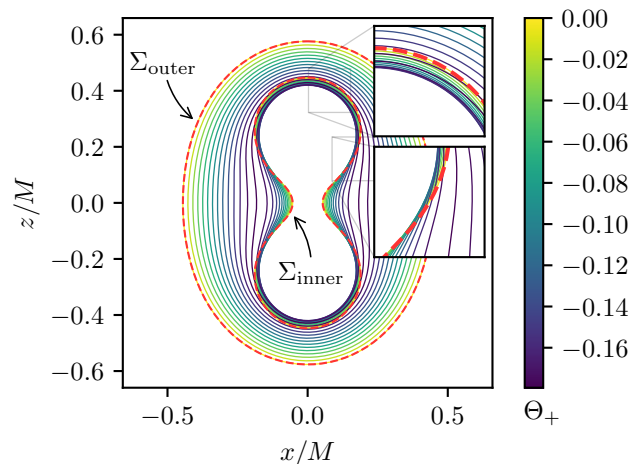
For multiple black holes, taking the absolute value of k yields results consistent with [43]. That is, for large spheres one recovers the ADM mass as expected while for small spheres approaching each puncture x_i, an asymptotic expansion yields the ADM mass associated to each puncture (19). Numerical calculation for CES around Σ_{outer} is also included in Fig. 5 (blue) and reveals a similar behavior as in the Schwarzschild case up to $\Theta_+ \approx -0.2$ where a turn-over happens in the multiple holes BL data (see below for discussion). Numerical calculation for CES toward each puncture, i.e. around $\Sigma_{A,B}$, is shown in Fig. 6 and again reveals a similar behavior as in the Schwarzschild case.

We emphasize that in Brill-Lindquist data, only CES families outside Σ_{outer} and inside each individual $\Sigma_{A,B}$ are comparable with the Schwarzschild case. The region bounded by Σ_{outer} surrounding all punctures and $\Sigma_{A,B}$ surrounding each individual puncture does not have a direct correspondence in the Schwarzschild case. The CES family interpolates between Σ_{outer} and the unstable common MOTS Σ_{inner} and does not approach either of the two asymptotic ends $x_{A,B}$ (Fig. 7). Moreover, in this region, constant expansion or constant mean curvature (CMC) surfaces fail to foliate space and monotonicity of the QLM indeed fails here. These explain peculiar features around Σ_{inner} in BL data seen in Fig. 5. We remark that choosing other families of foliating surfaces such as coordinate spheres yields qualitatively similar conclusions. The choice of families of CESs, which in time symmetry are constant mean curvature surfaces, allows us to get arbitrarily close to a MOTS, which is a CES itself.

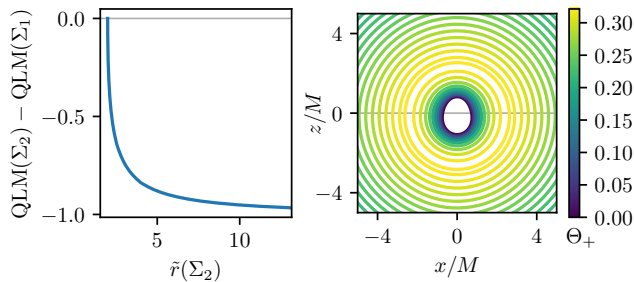Our extension confirms that QLM at the MOTS (16)

FIG. 8. Monotonicity of the QLM along a CES family going outward from $\Sigma_1 = \Sigma_{\text{outer}}$ at time $t = 2.5\,M$ in simulation Sim1. The area radius $\tilde{r}(\Sigma)$ increases monotonically along this family. The left panel shows the difference of the QLM between Σ_{outer} and Σ_2 as Σ_2 is moved outward. The right panel shows the region around Σ_{outer} foliated by the CES family.

should be

$$\text{QLM} = \frac{1}{8\pi} \int H_0 \geq 2\sqrt{\frac{|\Sigma|}{16\pi}} \qquad (35)$$

where $|\Sigma|$ denotes the area of Σ and the Minkowski inequality is invoked. This is already assumed in earlier studies [2].

B. QLM in non-time-symmetric slices

As one numerically evolves the time-symmetric initial data, the slices $\mathcal{S}$ become non-time-symmetric and the mean curvature vector of a surface $\Sigma \subset \mathcal{S}$ may acquire a timelike component. The Wang-Yau quasi-local mass will then in general differ from the Brown-York mass.

This has various consequences, one being that the monotonicity of the QLM along geometric flows is not guaranteed by (31) anymore, although we numerically find monotonicity remains true, as can be seen in Fig. 8. An analytic generalization of (31) to the non-time-symmetric case is under study.

1. QLM at a MOTS without time symmetry

In this section, we will numerically determine the QLM on CES families near Σ_{outer}. The goal is to justify the definition (16) of the QLM on a MOTS Σ by exploring its behavior as we approach Σ along the family from the $\Theta_+ > 0$ side, where the QLM is well defined.

Although ρ (8) and QLM (7) seem well-defined even for $|H| \to 0$, the OEE that determines τ is clearly singular at a MOTS: $|H|$ appears as denominator in both (9) and (27). Therefore, the definition of the QLM cannot trivially be extended to the case of a MOTS. In other words, as $\Theta_+ \to 0$, $|H| \to 0$, and so the assumption of having a spacelike mean curvature vector in the Wang-Yau QLM

breaks down. We focus on examining this issue here numerically. A mathematical treatment of this case will be given in Sec. VI.

To numerically explore what happens as $\Theta_+ \to 0$, we look at the individual terms in the OEE (9) that determines τ. As can be seen in Fig. 9, ρ remains finite while $\tau_\theta = \tau'$ approaches zero, so their product vanishes at a MOTS. Since $\tau' \to 0$, $\tau \to \text{const}$ and clearly $\alpha_{H_0} \to 0$. The remaining terms ψ_θ and α_H both remain finite in the limit. However, within numerical limits, they cancel in j_θ as $\Theta_+ \to 0$. The net result is thus $\tau \to 0$ is a solution to the OEE at a MOTS.

This suggests that as we approach a MOTS, τ becomes constant and j_a vanishes, so that $\rho \to |H_0|$. In terms of the QLM, this limit is shown in Fig. 10 together with the value of the QLM calculated at the MOTS using (16).

C. Time evolution of the QLM at a MOTS

Having argued that one can extend the Wang-Yau QLM to the common apparent horizon and each individual horizon by (16), we now examine its time evolution during the head-on merger of two black holes.

If one interprets the Wang-Yau QLM as a measure to separate quasi-local degrees of freedom from traveling gravitational waves, then Fig. 11 indicates the region surrounded by Σ_{outer} loses energy/mass while subregions surrounded by each individual horizon $\Sigma_{A,B}$ gain energy/mass during the collision. Furthermore, in the longer simulation Sim2, we find an oscillation in energy/mass contained inside the apparent horizon Σ_{outer} (Fig. 12). It is well known that for two black hole collisions, the intrinsic geometry of the apparent horizon experiences oscillations at the (lowest) quasi-normal frequency of the final black hole [64]. While the apparent horizon area monotonically increases despite the oscillation at the quasi-normal frequency, QLM of the apparent horizon fails to maintain monotonicity with the oscillation. Nevertheless, as the final black hole settles down to equilibrium, the measure of QLM and area for the apparent horizon converges.

First of all, although the Wang-Yau quasi-local mass is defined for a 2-surface and does not depend on the choice of slicing $\mathcal{S}$, determining the apparent horizon through Θ_+ does depend on the choice of slicing $\mathcal{S}$. Bearing in mind this ambiguity associated with the apparent horizon, one tends to conclude that the Wang-Yau quasi-local mass suggests that the region bounded by the outermost MOTS Σ_{outer} could lose energy to infinity. This is a different picture from that indicated by the area of the horizons, which increase monotonically, and the standard first law of black hole thermodynamics. This difference is actually expected: equation (6.20) in [16] indicates that the Brown-York quasi-local mass for a Schwarzschild black hole satisfies a balance equation that differs from the standard black hole thermodynamics. This again emphasizes that quasi-local mass as defined by Brown and
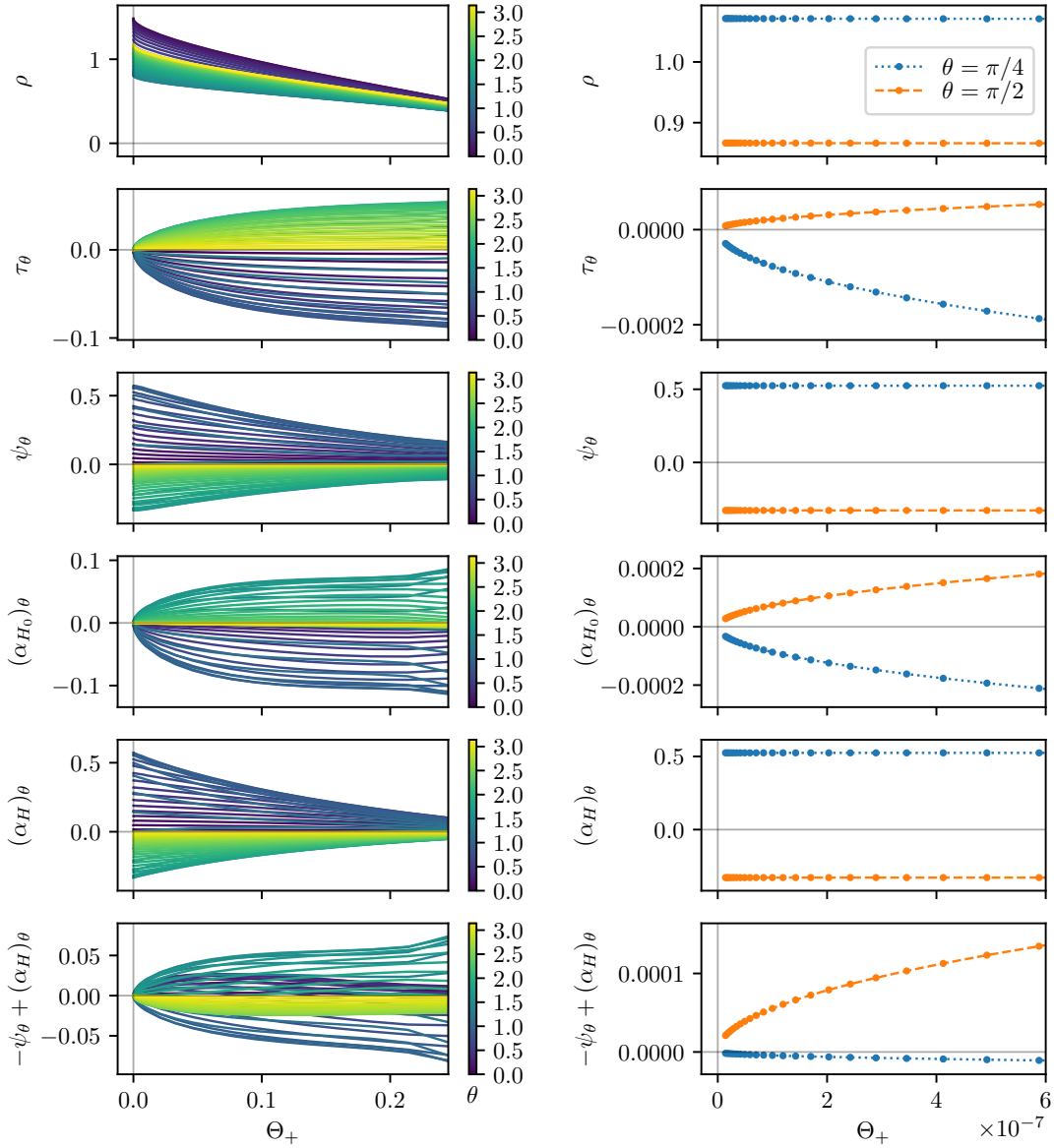
FIG. 9. Terms appearing in (9), i.e., $j_\theta = \rho\tau_\theta - \psi_\theta - (\alpha_{H_0})_\theta + (\alpha_H)_\theta$, where $\psi = \sinh^{-1}\left(\frac{\rho\Delta\tau}{|H_0||H|}\right)$. They are plotted as function of Θ_+ for CESs outside Σ_{outer}. For each curve, we fix the coordinate $\theta \in (0,\pi)$ along the surface and show its value as color. The right column is a close-up of $\Theta_+ = 0$ and depicts two individual values of θ. The first five rows show the individual quantities whereas the final row shows $-\psi_\theta + (\alpha_H)_\theta$. The slice is from Sim1 at time $t = 2.5\,M$.

York or Wang and Yau measures a different quantity than irreducible mass. More specifically, as the horizon expands, more negative gravitational field energy is taken into account by QLM which counteracts the positive contribution from growing area and absorbed gravitational waves. This issue is crucial in understanding Wang-Yau quasi-local mass and will be carefully studied with a direct calculation of gravitational wave energy in a future study.

1. Investigating the hoop-conjecture

A viable notion of QLM in general relativity should lead to numerous applications. We conclude this section on numerical results by exploring one such application, namely the hoop conjecture [65, 66]. This conjecture addresses the question of under what conditions a black hole forms. As we shall shortly see, several aspects of the conjecture are not precisely formulated and numerical relativity has a role to play in exploring and evaluating various possibilities; see e.g. [67] for recent work in this direction.

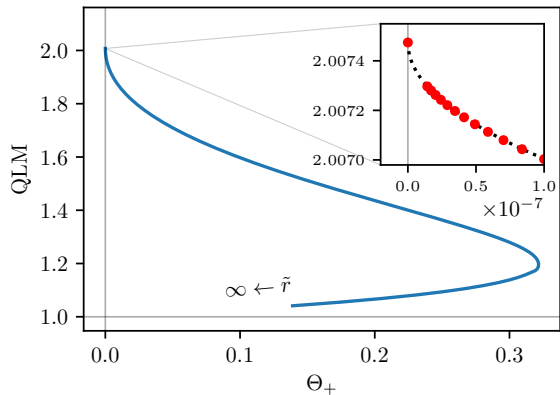In the case of gravitational collapse, the intuitive pic-

FIG. 10. QLM for CESs with $\Theta_+ > 0$ outside the MOTS Σ_{outer}. The value for Σ_{outer} at $\Theta_+ = 0$ is calculated using (16). The dotted line in the inset interpolates the data points (red) and is obtained by fitting $c_1 - c_2\sqrt{\Theta_+}$. The curve ends before reaching a QLM of 1 since the numerical slice does not extend to infinity. This is for simulation Sim1 at time $t = 2.5\,M$.
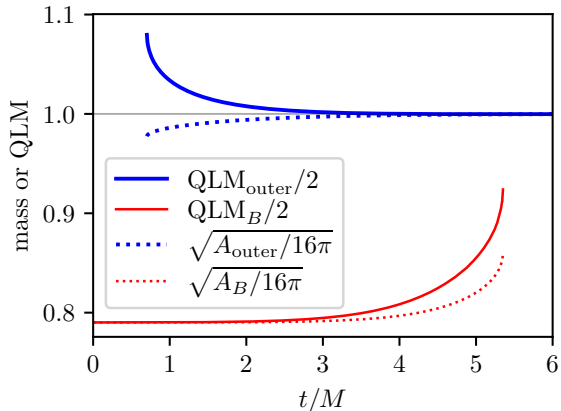

FIG. 11. QLM and area masses of Σ_{outer} and Σ_B calculated using (16) in simulation Sim1 as function of simulation time. The smaller horizon Σ_A (not shown) has a qualitatively similar behavior, though less pronounced, as Σ_B. For easier comparison, the QLM has been divided by 2 to account for the fact that for Schwarzschild, the QLM of the horizon is twice the ADM mass.

ture is that of matter fields getting compressed due to their self-gravity and eventually becoming sufficiently dense to form a black hole. As originally formulated by Kip Thorne: Horizons form when and only when a mass M gets compacted into a region whose circumference $\mathcal{C}$ in every direction does not exceed $4\pi GM/c^2$. Thus, in units with $G = c = 1$, a horizon should form when, and only when, $\mathcal{C}/4\pi M \lesssim 1$. Here the notion of what one means by mass is left vague, as is the space of curves ("hoops") one should use. Moreover, the value of 1 on the right hand side is motivated by the Schwarzschild metric, and other numerical values might be appropriate in general
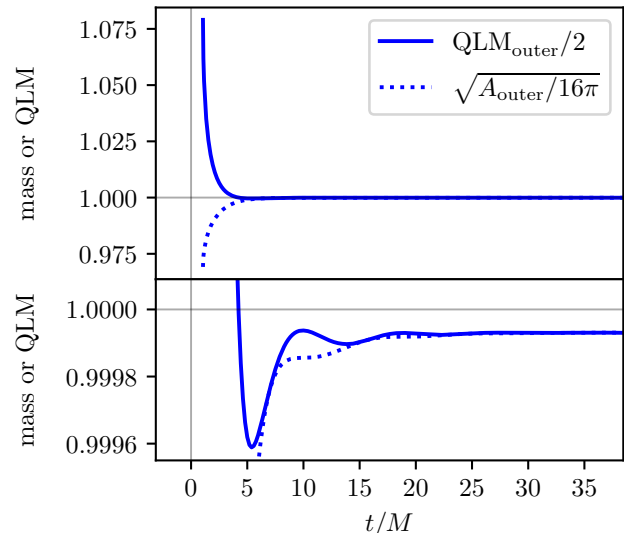

FIG. 12. Evolution of the QLM calculated using (16) on Σ_{outer} and the horizon's irreducible mass. This plot shows the longer simulation Sim2. At the final time, we have $\text{QLM}_{\text{outer}}/2 \approx 0.9999303$ and $\sqrt{A_{\text{outer}}/16\pi} \approx 0.9999309$. The lower panel is a close-up on the y-axis of the first panel.

situations.

If a notion of QLM is generally viable, it should be possible to use it as the appropriate mass within the hoop conjecture. For the Schwarzschild spacetime, as we have seen, the Wang-Yau QLM for the horizon is twice the ADM mass. Thus, one might expect the relevant hoop conjecture inequality should be modified to $\mathcal{C}/4\pi M < 0.5$. For the hoops, we shall use closed geodesics lying within the constant expansion surfaces that we have already found. In our present case, we do not deal with gravitational collapse, but rather with a binary black hole merger where we always have black holes present on any time slice. We instead seek to investigate the issue of when the common horizon forms, and whether its formation can be predicted by a hoop conjecture argument using the Wang-Yau QLM. We assume further that the hoop conjecture applies to the formation of marginally trapped surfaces. In our case, the constant expansion surfaces and the marginally trapped surfaces turn out to be prolate so that the polar circumference $\mathcal{C}_p$ is larger than the equatorial circumference. Thus we calculate the ratio $\mathcal{C}_p/4\pi M$ for constant expansion surfaces on different time slices in the vicinity of the time when the common horizon is first formed.

Our results are shown in Fig. 13. We see that the ratio $\mathcal{C}_p/4\pi M$ approaches 0.5 asymptotically as expected. At earlier times, this ratio is somewhat larger than the limiting value 0.5. This is not unusual – similar results were found in e.g. [67] where the ratio was about 12% larger than the limiting value predicted by the hoop conjecture. At each time just before the horizon is formed, the value of $\mathcal{C}_p/4\pi M$ approaches the limiting value as the expan-
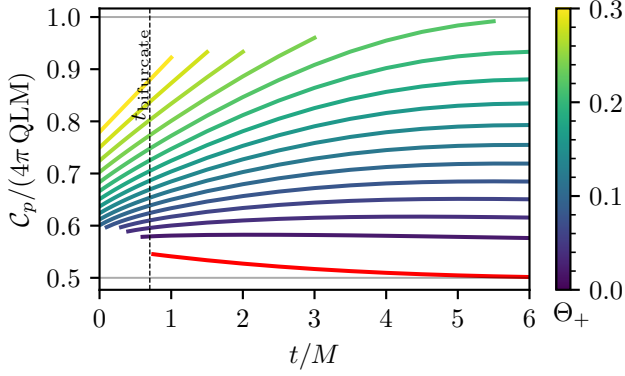
FIG. 13. Exploring the use of the Wang-Yau QLM in the hoop conjecture for the formation of the common horizon. The figure shows the ratio $\mathcal{C}_p/(4\pi \times \text{QLM})$ as functions of time for various constant expansion surfaces. The curve in red refers to the common horizon while the other curves refer to positive values of the expansion; the color scale indicates the values of the expansion, which lie apart by 0.02 at the color scale's ticks. The time labeled as $t_{\text{bifurcate}}$ is when the common horizon is formed.

sion becomes smaller. These results are suggestive but inconclusive – it is not yet clear whether this can be used as a prediction for the formation of the common horizon. This would require us to identify a suitable threshold for $\mathcal{C}_p/4\pi M$ for these surfaces. In the above discussion we have considered only the constant expansion surfaces. It is plausible that there exist other surfaces which have a smaller value of $\mathcal{C}_p/4\pi M$. Therefore, while we shall not do so here, it would be more satisfactory to consider a more general class of 2-spheres and to minimize the ratio $\mathcal{C}_p/4\pi M$ over these spheres. Following the spirit of the hoop conjecture, one could then look for a threshold on this minimum value of $\mathcal{C}_p/4\pi M$, and investigate whether it can predict the formation of a black hole horizon.

VI. DEFINING THE QLM ON A MOTS

The above numerical results have already used a "working definition" (16) for evaluating the Wang-Yau QLM on a MOTS. In this section, we explore the limit $\Theta_+ \to 0$ from a mathematical perspective to justify this definition. It seems plausible that an extension to the case with angular momentum is possible. However, this will be left to future work.

Lemma VI.1. *Consider an axisymmetric collision with no angular momentum involved. Further assume isometric embedding or time function τ being axisymmetric, then $j \equiv 0$ when it is well-defined, i.e. when the mean curvature vector H is spacelike.*

Proof. Use the definition (9). We first observe that under the above assumptions, $j_\phi \equiv 0$. It is easy to see that

$\nabla_{\partial_\phi}\tau = \nabla_\phi\left(\sinh^{-1}\frac{\rho\Delta\tau}{|H_0||H|}\right) = 0$ by assumption. That connection one-forms vanish can be seen from computing Christoffel symbols, using subscripts $3, 4$ for the H and J direction,

$$\Gamma^4_{\phi 3} = \frac{1}{2}g^{4\mu}\left(\partial_\phi(g_{3\mu}) + \partial_3(g_{\phi\mu}) - \partial_\mu(g_{\phi 3})\right)$$
$$= \frac{1}{2}g^{4\mu}\,\partial_3(g_{\phi\mu})$$

and noting that the spacetime under consideration possesses a symmetry $\phi \to -\phi$ such that cross terms in the metric involving ϕ all vanish.

Next we show $j_\theta = 0$. The most general axisymmetric metric for a 2-surface is

$$d\sigma^2 = r_0^2 P(r_0, \theta)^2 d\theta^2 + r_0^2 Q(r_0, \theta)^2 \sin^2\theta d\phi^2 \ .$$

Then

$$\nabla_a j^a = \frac{1}{\sqrt{\sigma}}\partial_\theta(\sqrt{\sigma}\sigma^{\theta\theta}j_\theta) = \frac{1}{\sqrt{\sigma}}\partial_\theta(\frac{Q}{P}\sin\theta\, j_\theta) = 0$$

$$\frac{Q}{P}\sin\theta\, j_\theta = \text{const} \ .$$

Using that Q, P do not vanish (metric non-degenerate), $\sin(0) = \sin(\pi) = 0$ and that j is well-defined, one gets const $= 0$ and hence $j_\theta \equiv 0$ on the surface.

$\square$

Remark VI.2. *This may sound contradictory to the well-known fact that there are infinitely many non-vanishing, smooth, divergence-free vector fields on S^2. We elaborate on this. Denote the volume form by $\omega = \sqrt{\sigma}d\theta \wedge d\phi$. Take divergence-free vector field $j = j^\theta\partial_\theta$ with $j^\phi = 0$. Then*

$$\text{div}(j)\omega = \mathcal{L}_j\omega = d\iota_j\omega = 0 \ .$$

Given that $H^1_{dR}(S^2) = 0$, there exist a smooth function $f(\theta, \phi)$ such that $\iota_j\omega = df$. That is,

$$r_0^2 PQ\sin\theta\, j^\theta d\phi = df = \frac{\partial f}{\partial\theta}d\theta + \frac{\partial f}{\partial\phi}d\phi \ .$$

It follows that $\frac{\partial f}{\partial\theta} = 0$. Then noting that the RHS is only a function of ϕ while the LHS clearly has a dependence on θ, it follows that $j^\theta = f = 0$. We again reach $j \equiv 0$ when axisymmetry is imposed.

Remark VI.3. *When angular momentum is present, the metric would have cross terms involving ϕ and the connection one-form α_H would generally not vanish ($\alpha_{H_0} = 0$ since the reference spacetime is static). In fact, the quasi-local angular momentum as defined in [23] vanishes exactly when $j^\phi = 0$, consistent with our proof above. Recall that quasi-local angular momentum is defined as*

$$E(\Sigma, X, T_0, K = \partial_\phi) = -\frac{1}{8\pi}\int \langle K, T_0\rangle\rho + K^a j_a \ .$$

If one assumes Σ and τ both axisymmetric, $\langle K, T_0\rangle = 0$. $E(\Sigma, X, T_0, K = \partial_\phi) = 0$ if and only if $j^\phi = 0$.

Theorem VI.4. *Assume H_0 remains spacelike as H turns into null or $|H| \to 0$, then the solution τ to the OEE approaches a constant as the surface approaches the apparent horizon.*

Proof. Note that $H_0 = \hat{k}\check{e}_3 + \frac{\Delta\tau}{\sqrt{1+|\nabla\tau|^2}}\check{e}_4$, where $\hat{k}$ is the mean curvature of the projected surface $\pi(i_0(\Sigma))$ in $\mathbb{R}^3$, with $\pi : \mathbb{R}^{3,1} \to \mathbb{R}$ being projection along T_0. Assuming H_0 remains spacelike thus implies that τ is well behaved since otherwise $\frac{\Delta\tau}{|\nabla\tau|} \to \infty$ and H_0 is surely timelike.

Having proved that $j \equiv 0$ as $|H| \to 0$, we next examine (9) term by term to show that $\nabla_a\big(\sinh^{-1}\frac{\rho\Delta\tau}{|H||H_0|}\big)$ needs to be bounded, which in turn leads to $\Delta\tau \to 0$ and hence $\tau \to$ const as $|H| \to 0$.

First look at the α_H term. Use (27) and the fact that the family of Σ is constant expansion surface with $\partial_a\Theta_+ \equiv 0$,

$$\alpha_H = \frac{1}{2}\left(-\frac{\partial_a\Theta_-}{\Theta_-} - \langle {}^{(4)}\nabla_a\ell_-, \ell_+\rangle\right)$$

and hence bounded as $\theta_+ \to 0$.

Next look at the α_{H_0} term. Using $\check{e}_4 = \frac{T_0+\nabla\tau}{\sqrt{1+|\nabla\tau|^2}}$ and $\langle {}^{(4)}\nabla_a\check{e}_3, T_0\rangle = 0$

$$\alpha_{H_0}(e_a) = \langle {}^{(3,1)}\nabla_a\check{e}_3, \check{e}_4\rangle = II\left(e_a, \frac{\nabla\tau}{\sqrt{1+|\nabla\tau|^2}}\right),$$

where II is the second fundamental form of the cylinder spanned by $i_0(\Sigma)$ and T_0 in $\mathbb{R}^{3,1}$. Therefore α_{H_0} is also bounded as $\theta_+ \to 0$.

Lastly, note that

$$\rho\nabla\tau = \left(\sqrt{|H_0|^2 + \frac{(\Delta\tau)^2}{1+|\nabla\tau|^2}} - \sqrt{|H|^2 + \frac{(\Delta\tau)^2}{1+|\nabla\tau|^2}}\right)$$
$$\times \frac{\nabla\tau}{\sqrt{1+|\nabla\tau|^2}}$$

also remains bounded as $\theta_+ \to 0$.

Putting together, one sees that $\nabla_\theta\left(\sinh^{-1}\frac{\rho\Delta\tau}{|H||H_0|}\right)$ has to remain finite for $j \equiv 0$ as $|H| \to 0$. This is only possible when $\Delta\tau \to 0$ as $|H| \to 0$, i.e. $\tau \to$ const.

To gain more understanding about the limit $\tau \to$ const, we use another formula for j that does not invoke picking the specific frame $\{e_H, e_J\}$

$$j = \rho\nabla\tau - \alpha_{\check{e}_3} + \alpha_{\overline{e}_3}.$$

Indeed,

$$-\alpha_{H_0} + \alpha_H - \nabla\left(\sinh^{-1}\frac{\rho\Delta\tau}{|H||H_0|}\right)$$
$$= -\alpha_{H_0} - \nabla\psi_0 + \alpha_H + \nabla\psi$$
$$= -\alpha_{\check{e}_3} + \alpha_{\overline{e}_3}.$$

Imposing $\tau = $ const, $\rho\nabla\tau = 0$ and $\alpha_{\check{e}_3} = \langle {}^{(3,1)}\nabla\check{e}_3, \check{e}_4\rangle = 0$, recalling that $\check{e}_4 = \frac{T_0+\nabla\tau}{\sqrt{1+|\nabla\tau|^2}}$. One

is left with $\alpha_{\overline{e}_3}$ only. Recall that $\overline{e}_3$ is the 'spacelike' unit normal chosen by the gauge condition

$$\langle\overline{e}_4, H\rangle = \langle\check{e}_4, H_0\rangle,$$

which vanishes for $\tau = $ const or $i_0(\Sigma) \subset \mathbb{R}^3$. When H is spacelike, this gauge condition picks $\overline{e}_3 \propto H$ and $\alpha_{\overline{e}_3} = \alpha_H$ which in general do not vanish. So $\tau = $ const does not solve OEE in general.

Now consider the limit $\Theta_+ \to 0$. Since

$$H = \frac{\Theta_+\ell_- + \Theta_-\ell_+}{2}, \quad J = \frac{\Theta_+\ell_- - \Theta_-\ell_+}{2}$$

as $\Theta_+ \to 0$, H and J both turn to null vectors along ℓ_+. The gauge condition $\langle\overline{e}_4, H\rangle = 0$ forces $\overline{e}_4, \overline{e}_3 \propto \ell_+$. Thus $\alpha_{\overline{e}_3} = \langle\nabla\overline{e}_3, \overline{e}_4\rangle = 0$ and $j = 0$ is satisfied. $\square$

Remark VI.5. *The above proposition shows that one can extrapolate the definition of the QLM to $|H| = 0$ with the optimal embedding being $\tau = $ const. In this case, i.e. $\tau = $ const and $|H| = 0$,*

$$\mathrm{QLM} = \frac{1}{8\pi}\int\rho$$
$$= \frac{1}{8\pi}\int\frac{\sqrt{|H_0|^2 + \frac{(\Delta\tau)^2}{1+|\nabla\tau|^2}} - \sqrt{|H|^2 + \frac{(\Delta\tau)^2}{1+|\nabla\tau|^2}}}{\sqrt{1+|\nabla\tau|^2}}$$
$$= \frac{1}{8\pi}\int|H_0|.$$

Remark VI.6. *As proved in [28], a solution τ to the optimal embedding equation is a local minimum of Wang-Yau quasi-local energy if*

$$|H_\tau| > |H| > 0,$$

where H_τ is the mean curvature vector of the isometric embedding with time function τ. The condition is satisfied for constant expansion surfaces with $\Theta_+ > 0$ (Fig. 14). Assume continuity, $\tau = $ const is a local minimum of Wang-Yau quasi-local energy at the apparent horizon.

The numerical calculations in Sec. V B 1 comply with the above results.

VII. CONCLUSIONS

In this work, we have studied the Wang-Yau quasi-local mass during a binary black hole merger. The Wang-Yau QLM uses an embedding of 2-surfaces in Minkowski space. We have solved the optimal embedding equation numerically and applied it to the head-on collision of two non-spinning black holes starting with Brill-Lindquist initial data. We numerically determined the QLM for surfaces close to the horizons and for families of surfaces approaching the asymptotically flat ends and study their
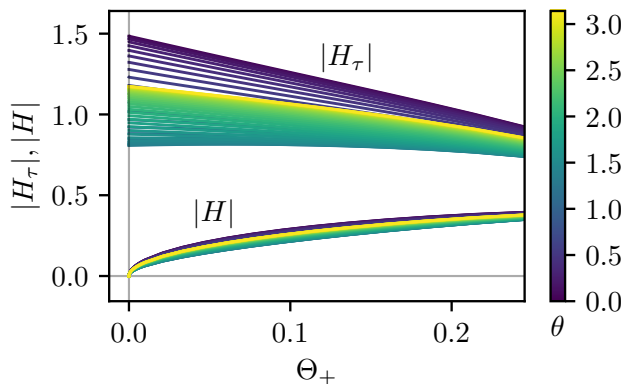
FIG. 14. Value of $|H_\tau|$ and $|H|$ along the CESs outside Σ_{outer} at simulation time $t = 2.5\,M$ in Sim1. As Fig. 9, the colors indicate the coordinates on the surface.

time evolution, and also present a preliminary investigation of the hoop conjecture applied to the formation of the common horizon. Finally, we have suggested an extension of the Wang-Yau QLM to marginally trapped surfaces.

For a Schwarzschild black hole, our calculations agree with the well known result of the Brown-York mass, i.e. the QLM is twice the ADM mass on the horizon. The Brown-York mass decreases monotonically as one moves outward from the horizon, and for the sphere at infinity, it yields the ADM mass. This is in sharp contrast to other quasi-local mass definitions such as Hawking and Bartnik masses. The Wang-Yau quasi-local mass also inherits this monotonic decreasing property. Such monotonicity is clearly demonstrated numerically for our family of constant expansion surfaces. Therefore, it is a crucial property of the Wang-Yau quasi-local mass that some measure of negative gravitational field energy is accounted for. In particular, for surfaces Σ in a time-symmetric slice $\mathcal{S}$, an explicit expression for gravitational field energy was written down [57]. An analogous expression for the case of non-time-symmetric slices is under study.

We have extended the definition of Wang-Yau quasi-local mass for 2-surfaces of spacelike mean curvature vector to 2-surfaces of null mean curvature vector, i.e. (16). With this extension, we examined the time evolution of QLM for a black hole, defined as QLM at Σ_{outer}, during the head-on collision of two non-spinning black holes. As is well known, the area increases monotonically throughout the evolution. At late stages, the area evolution exhibits damped oscillations which are known to be associated with the quasi-normal modes of the remnant black

hole (see e.g. [68]). In contrast, QLM decreases monotonically at first and starts to lose monotonicity when oscillations take place. We see from the bottom panel of Fig. 12 that the oscillation frequency of the QLM is similar to that of the area and one might expect these to also be associated with the quasi-normal modes. Monotonicity could be included as one of the additional requirements for a QLM, and in future work we shall investigate the possibility to modifying the definition of the QLM appropriately to make it monotonic.

That QLM and area evolve differently seems to comply with a variation equation for the Brown-York mass in the Schwarzschild black hole case [16], which differs from the standard first law of black hole thermodynamics. One might again invoke negative gravitational field energy to explain this difference. Nevertheless, both of these measures, namely the area and half of QLM of the apparent horizon converge to the same value asymptotically as the final black hole settles down to its equilibrium state. We expect that employing estimates of gravitational wave energy will greatly clarify on various distinctive features of the Wang-Yau quasi-local energy.

Future work will extend this study in various directions. Further extension of quasi-local definition for mass and angular momentum to surfaces of time-like mean curvature vector is of great interest. An example is trapped surfaces inside the horizon, whose quasi-local mass might reveal important information about black holes. An attempt definition based on Brown-York mass was made in a previous study [17], where it is found the quasi-local mass either experiences an infinite slope or a cusp at the horizon while the former was preferred by those authors. A naive extension of Wang-Yau QLM presented here reveals a similar behavior. A careful study of this issue will be presented elsewhere.

Furthermore, it will be important to calculate the QLM in cases with rotation or angular momentum. In these cases, we can also calculate the quasi-local angular momentum. Quasiloal mass and angular momentum for surfaces inside Kerr's ergoregion might exhibit interesting features related to the Penrose process. The time variation of the mass and angular momentum should be related to appropriate fluxes. Moreover, the event horizon, whose determination requires the knowledge of the whole spacetime evolution, may reveal different information from the apparent horizon studied here. Finally, an extension of the QLM and angular momentum to cosmological spacetimes would be of great interest. Here it would be necessary to consider a reference configuration not in Minkowski spacetime, but in de Sitter or anti-de Sitter spacetime [69].

[1] R. Penrose, Some unsolved problems in classical general relativity, in *Seminar on Differential Geometry. (AM-102), Volume 102*, edited by S.-T. Yau (Princeton University Press, Princeton, 1982) pp. 631–668.

[2] L. B. Szabados, Quasi-local energy-momentum and angular momentum in general relativity, Living reviews in

relativity **12**, 1 (2009).

[3] R. L. Arnowitt, S. Deser, and C. W. Misner, Dynamical Structure and Definition of Energy in General Relativity, Phys. Rev. **116**, 1322 (1959).

[4] R. Schoen and S.-T. Yau, Positivity of the Total Mass of a General Space-Time, Phys. Rev. Lett. **43**, 1457 (1979).

[5] E. Witten, A Simple Proof of the Positive Energy Theorem, Commun. Math. Phys. **80**, 381 (1981).

[6] H. Bondi, M. G. J. van der Burg, and A. W. K. Metzner, Gravitational waves in general relativity. 7. Waves from axisymmetric isolated systems, Proc. Roy. Soc. Lond. A **269**, 21 (1962).

[7] A. Ashtekar and B. Krishnan, Dynamical horizons: Energy, angular momentum, fluxes and balance laws, Phys. Rev. Lett. **89**, 261101 (2002), arXiv:gr-qc/0207080.

[8] A. Ashtekar and B. Krishnan, Dynamical horizons and their properties, Phys. Rev. D **68**, 104030 (2003), arXiv:gr-qc/0308033.

[9] E. Gourgoulhon and J. L. Jaramillo, Area evolution, bulk viscosity and entropy principles for dynamical horizons, Phys. Rev. D **74**, 087502 (2006), arXiv:gr-qc/0607050.

[10] C.-C. M. Liu and S.-T. Yau, Positivity of quasi-local mass II, Journal of the American Mathematical Society **19**, 181 (2006).

[11] M.-T. Wang and S.-T. Yau, Quasilocal mass in general relativity, Phys. Rev. Lett. **102**, 021101 (2009), arXiv:0804.1174 [gr-qc].

[12] C.-C. M. Liu and S.-T. Yau, Positivity of quasilocal mass, Phys. Rev. Lett. **90**, 231102 (2003).

[13] R. Bartnik, New definition of quasilocal mass, Phys. Rev. Lett. **62**, 2346 (1989).

[14] S. Hawking, Gravitational radiation in an expanding universe, J. Math. Phys. **9**, 598 (1968).

[15] R. Penrose, Quasilocal mass and angular momentum in general relativity, Proc. Roy. Soc. Lond. A **381**, 53 (1982).

[16] J. D. Brown and J. W. York, Jr., Quasilocal energy and conserved charges derived from the gravitational action, Phys. Rev. D **47**, 1407 (1993), arXiv:gr-qc/9209012.

[17] A. P. Lundgren, B. S. Schmekel, and J. W. York Jr, Self-renormalization of the classical quasilocal energy, Physical Review D **75**, 084026 (2007).

[18] J. Kijowski, A Simple Derivation of Canonical Structure and Quasi-local Hamiltonians in General Relativity, General Relativity and Gravitation **29**, 307 (1997).

[19] Y. Shi and L.-F. Tam, Positive Mass Theorem and the Boundary Behaviors of Compact Manifolds with Nonnegative Scalar Curvature, Journal of Differential Geometry **62**, 79 (2002).

[20] M.-T. Wang and S.-T. Yau, Isometric embeddings into the minkowski space and new quasi-local mass, Communications in Mathematical Physics **288**, 919 (2009).

[21] M.-T. Wang and S.-T. Yau, Limit of quasilocal mass at spatial infinity, Communications in Mathematical Physics **296**, 271 (2010).

[22] P. Chen, M.-T. Wang, and S.-T. Yau, Evaluating quasilocal energy and solving optimal embedding equation at null infinity, Communications in mathematical physics **308**, 845 (2011).

[23] P.-N. Chen, M.-T. Wang, and S.-T. Yau, Conserved quantities in general relativity: from the quasi-local level to spatial infinity, Communications in Mathematical Physics **338**, 31 (2015).

[24] P.-N. Chen, J. Keller, M.-T. Wang, Y.-K. Wang, and S.-T. Yau, Evolution of angular momentum and center of mass at null infinity, Communications in Mathematical Physics **386**, 551 (2021).

[25] P.-N. Chen, M.-T. Wang, Y.-K. Wang, and S.-T. Yau, Supertranslation invariance of angular momentum, arXiv preprint arXiv:2102.03235 (2021).

[26] P.-N. Chen, M.-T. Wang, Y.-K. Wang, and S.-T. Yau, Supertranslation invariance of angular momentum at null infinity in double null gauge, arXiv preprint arXiv:2204.03182 (2022).

[27] P.-N. Chen, M.-T. Wang, and S.-T. Yau, Evaluating quasilocal energy and solving optimal embedding equation at null infinity, Commun. Math. Phys. **308**, 845 (2011), arXiv:1002.0927 [math.DG].

[28] P.-N. Chen, M.-T. Wang, and S.-T. Yau, Minimizing properties of critical points of quasi-local energy, Communications in Mathematical Physics **329**, 919 (2014).

[29] A. Ashtekar and B. Krishnan, Isolated and dynamical horizons and their applications, Living Rev. Rel. **7**, 10 (2004), arXiv:gr-qc/0407042.

[30] I. Booth, Black hole boundaries, Can. J. Phys. **83**, 1073 (2005), arXiv:gr-qc/0508107.

[31] E. Gourgoulhon and J. L. Jaramillo, A 3+1 perspective on null hypersurfaces and isolated horizons, Phys. Rept. **423**, 159 (2006), arXiv:gr-qc/0503113.

[32] S. A. Hayward, Energy and entropy conservation for dynamical black holes, Phys. Rev. **D70**, 104027 (2004), arXiv:gr-qc/0408008.

[33] J. L. Jaramillo, An introduction to local Black Hole horizons in the 3+1 approach to General Relativity, Int. J. Mod. Phys. **D20**, 2169 (2011), arXiv:1108.2408 [gr-qc].

[34] L. Andersson, M. Mars, and W. Simon, Local existence of dynamical and trapping horizons, Phys.Rev.Lett. **95**, 111102 (2005), arXiv:gr-qc/0506013 [gr-qc].

[35] L. Andersson, M. Mars, and W. Simon, Stability of marginally outer trapped surfaces and existence of marginally outer trapped tubes, Adv.Theor.Math.Phys. **12** (2008), arXiv:0704.2889 [gr-qc].

[36] L. Andersson and J. Metzger, The area of horizons and the trapped region, Communications in Mathematical Physics **290**, 941 (2009).

[37] D. Pook-Kolb, O. Birnholtz, B. Krishnan, and E. Schnetter, Interior of a Binary Black Hole Merger, Phys. Rev. Lett. **123**, 171102 (2019), arXiv:1903.05626 [gr-qc].

[38] D. Pook-Kolb, O. Birnholtz, B. Krishnan, and E. Schnetter, Self-intersecting marginally outer trapped surfaces, Phys. Rev. D **100**, 084044 (2019), arXiv:1907.00683 [gr-qc].

[39] D. Pook-Kolb, O. Birnholtz, J. L. Jaramillo, B. Krishnan, and E. Schnetter, Horizons in a binary black hole merger I: Geometry and area increase, arXiv:2006.03939 [gr-qc] (2020).

[40] D. Pook-Kolb, R. A. Hennigar, and I. Booth, What Happens to Apparent Horizons in a Binary Black Hole Merger?, Phys. Rev. Lett. **127**, 181101 (2021), arXiv:2104.10265 [gr-qc].

[41] D. Pook-Kolb, I. Booth, and R. A. Hennigar, Ultimate fate of apparent horizons during a binary black hole merger. II. The vanishing of apparent horizons, Phys. Rev. D **104**, 084084 (2021), arXiv:2104.11344 [gr-qc].

[42] I. Booth, R. A. Hennigar, and D. Pook-Kolb, Ultimate fate of apparent horizons during a binary black hole merger. I. Locating and understanding axisymmetric marginally outer trapped surfaces, Phys. Rev. D **104**,

084083 (2021), arXiv:2104.11343 [gr-qc].

[43] D. R. Brill and R. W. Lindquist, Interaction energy in geometrostatics, Physical Review **131**, 471 (1963).

[44] D. Pook-Kolb, O. Birnholtz, B. Krishnan, and E. Schnetter, Existence and stability of marginally trapped surfaces in black-hole spacetimes, Phys. Rev. D **99**, 064005 (2019), arXiv:1811.10405 [gr-qc].

[45] M. Ansorg, B. Brügmann, and W. Tichy, A single-domain spectral method for black hole puncture data, Phys. Rev. D **70**, 064011 (2004), arXiv:gr-qc/0404056.

[46] F. Löffler, J. Faber, E. Bentivegna, T. Bode, P. Diener, R. Haas, I. Hinder, B. C. Mundim, C. D. Ott, E. Schnetter, G. Allen, M. Campanelli, and P. Laguna, The Einstein Toolkit: A Community Computational Infrastructure for Relativistic Astrophysics, Class. Quantum Grav. **29**, 115001 (2012), arXiv:1111.3344 [gr-qc].

[47] EinsteinToolkit, Einstein Toolkit: Open software for relativistic astrophysics, http://einsteintoolkit.org/.

[48] J. D. Brown, P. Diener, O. Sarbach, E. Schnetter, and M. Tiglio, Turduckening black holes: an analytical and computational study, Phys. Rev. D **79**, 044023 (2009), arXiv:0809.3533 [gr-qc].

[49] S. Husa, I. Hinder, and C. Lechner, Kranc: a Mathematica application to generate numerical codes for tensorial evolution equations, Comput. Phys. Commun. **174**, 983 (2006), arXiv:gr-qc/0404023.

[50] Kranc, Kranc: Kranc assembles numerical code.

[51] M. Alcubierre, G. Allen, B. Brügmann, T. Dramlitsch, J. A. Font, P. Papadopoulos, E. Seidel, N. Stergioulas, W.-M. Suen, and R. Takahashi, Towards a stable numerical evolution of strongly gravitating systems in general relativity: The Conformal treatments, Phys. Rev. **D62**, 044034 (2000), arXiv:gr-qc/0003071 [gr-qc].

[52] M. Alcubierre, B. Brügmann, P. Diener, M. Koppitz, D. Pollney, E. Seidel, and R. Takahashi, Gauge conditions for long term numerical black hole evolutions without excision, Phys. Rev. **D67**, 084023 (2003), arXiv:gr-qc/0206072 [gr-qc].

[53] D. Pook-Kolb, O. Birnholtz, I. Booth, R. A. Hennigar, J. L. Jaramillo, B. Krishnan, E. Schnetter, and V. Zhang, Mots finder version 1.5 (2021).

[54] J. Boyd, *Chebyshev and Fourier Spectral Methods* (Dover Publications, New York, 2001).

[55] A. Meurer, C. P. Smith, M. Paprocki, O. Čertík, S. B. Kirpichev, M. Rocklin, A. Kumar, S. Ivanov, J. K. Moore, S. Singh, *et al.*, SymPy: symbolic computing in Python, PeerJ Computer Science **3**, e103 (2017).

[56] E. A. Martinez, Quasilocal energy for a kerr black hole, Physical Review D **50**, 4920 (1994).

[57] P. Miao, Y. Shi, and L.-F. Tam, On geometric problems related to brown-york and liu-yau quasilocal mass, Communications in mathematical physics **298**, 437 (2010).

[58] G. Huisken and S.-T. Yau, Definition of center of mass for isolated physical systems and unique foliations by stable spheres with constant mean curvature, Inventiones mathematicae **124**, 281 (1996).

[59] J. Qing and G. Tian, On the uniqueness of the foliation of spheres of constant mean curvature in asymptotically flat 3-manifolds, Journal of the American Mathematical Society **20**, 1091 (2007).

[60] J. Metzger, Foliations of asymptotically flat 3-manifolds by 2-surfaces of prescribed mean curvature, Journal of Differential Geometry **77**, 201 (2007).

[61] L.-H. Huang, Foliations by stable spheres with constant mean curvature for isolated systems with general asymptotics, Communications in Mathematical Physics **300**, 331 (2010).

[62] C. Nerz, Foliations by stable spheres with constant mean curvature for isolated systems without asymptotic symmetry, Calculus of Variations and Partial Differential Equations **54**, 1911 (2015).

[63] M. Eichmair and T. Koerber, Foliations of asymptotically flat 3-manifolds by stable constant mean curvature spheres, arXiv preprint arXiv:2201.12081 (2022).

[64] P. Anninos, D. Bernstein, S. R. Brandt, D. Hobill, E. Seidel, and L. Smarr, Dynamics of black hole apparent horizons, Physical Review D **50**, 3801 (1994).

[65] K. Thorne, MAGIC WITHOUT MAGIC - JOHN ARCHIBALD WHEELER. A COLLECTION OF ESSAYS IN HONOR OF HIS 60TH BIRTHDAY (Freeman, San Francisco, 1972) p. 231.

[66] J. M. M. Senovilla, A Reformulation of the Hoop Conjecture, EPL **81**, 20004 (2008), arXiv:0709.0695 [gr-qc].

[67] E. Ames, H. Andréasson, and O. Rinne, On the Hoop conjecture and the weak cosmic censorship conjecture for the axisymmetric Einstein-Vlasov system, arXiv:2305.04360 [gr-qc] (2023).

[68] P. Mourier, X. Jiménez Forteza, D. Pook-Kolb, B. Krishnan, and E. Schnetter, Quasinormal modes and their overtones at the common horizon in a binary black hole merger, Phys. Rev. D **103**, 044054 (2021), arXiv:2010.15186 [gr-qc].

[69] P.-N. Chen, M.-T. Wang, and S.-T. Yau, Quasi-local energy with respect to de sitter/anti-de sitter reference, arXiv preprint arXiv:1603.02975 (2016).